DeltaVs: A Method for Detecting Significant Layer Boundaries in Surface Wave Inversion Results

Michael B. S. Yust, S.M.ASCE[1]; and Brady R. Cox, Ph.D., P.E., M.ASCE[2]

Abstract: Surface wave testing is a powerful tool for noninvasive seismic site characterization. It includes a wide variety of active-source and passive-wavefield methods [e.g., spectral analysis of surface waves (SASW), multichannel analysis of surface waves (MASW), microtremor array measurements (MAM)] that can be applied to many different field conditions. The dispersion data collected with all these methods can be inverted to produce (one-dimensional) 1D shear wave velocity (V_S) profiles of the subsurface. A critical part of this inversion procedure is the need to develop several trial model parameterizations with different numbers of layers as a means for investigating epistemic uncertainty and nonuniqueness when attempting to fit the experimental dispersion data. This is especially important when a priori information either is not available or does not extend to great enough depths to constrain the inversions. These trial parameterizations are used to vary the number of potential layers present in the subsurface models and to set the acceptable search ranges for depths to boundaries and stiffness in each layer. The inversion results are highly affected by the parameterizations. When performing high-quality inversions, it is important to use different parameterization options to fully explore potential conditions at the site and characterize the epistemic uncertainty of the inversion process. While this practice allows for a robust analysis of the experimental dispersion data and its uncertainty, it also generates many potential subsurface models for the site, which can represent a challenge for engineers when deciding which V_S profiles best represent the true subsurface layering for use in subsequent analysis and design (e.g., seismic site response). This paper presents an approach, called the DeltaVs method, for systematically evaluating the depths of layer boundaries across all acceptable models determined from several different inversion layering parameterizations as a means to identify distinct clusters of boundaries. Using these clusters, the number and location of meaningful layer boundaries can be determined for many sites, thereby allowing for the elimination of some parameterization options containing more, or fewer, boundaries and a reduction in epistemic uncertainty. The distributions of layer boundaries within these clusters can then be used to determine statistics for the depths of layer boundaries that are consistent with the epistemic uncertainty of the models produced by the inversion procedure. The DeltaVs method is demonstrated on 12 synthetic ground models as well as one field data set. **DOI: 10.1061/JGGEFK.GTENG-10893.**

Introduction

Surface wave testing is a powerful tool for noninvasive seismic site characterization. It comprises a wide variety of active-source and passive-wavefield methods [e.g., spectral analysis of surface waves (SASW), multichannel analysis of surface waves (MASW), microtremor array measurements (MAM)] that can be applied to many different field conditions. While the exact procedures for collecting and analyzing data using these methods may differ, they all consist of the same three general steps: field data acquisition of stress waves with strong surface wave content, processing of the waveforms to extract experimental dispersion data, and inversion of the experimental dispersion data to obtain one-dimensional (1D) subsurface velocity models (Foti et al. 2015). Field data acquisition involves recording wavefields at the surface of the site generated during the test (active) and/or by external phenomena (passive). Active sources range from simply striking the ground with a hammer, to more complex devices such as a vibroseis shaker. Passive noise sources include natural phenomena such as wind, ocean waves, or seismic microtremors, as well as anthropogenic sources such as nearby traffic or industrial activity.

The processing stage involves transforming the wavefield data into surface wave dispersion data (Zywicki 1999). The dispersion data sets from individual acquisition methods and source locations can then be combined statistically into a single data set that shows site-specific behavior (i.e., mean and standard deviation) of surface wave phase velocity as a function of frequency and/or wavelength. This statistical representation of dispersion data contains both aleatory and epistemic sources of uncertainty. Aleatory variability is included in the dispersion data due to inherent spatial variability in the soils beneath the surface wave arrays. Epistemic uncertainty is included in the dispersion data due to choices made during data collection and processing (e.g., various wavefield transform methods). The combined effects of aleatory variability and epistemic uncertainty on the dispersion data are effectively impossible to decouple (Griffiths et al. 2016; Teague and Cox 2016) and are often simply referred to as dispersion uncertainty in the literature (e.g., Lai et al. 2005; Foti et al. 2009; Cox and Wood 2011; Teague et al. 2018; Yust et al. 2018; Vantassel and Cox 2022). This overall dispersion uncertainty is generally believed to be normally distributed and should be propagated through to the final inversion results when possible (Lai et al. 2005; Vantassel and Cox 2021a).

The third and final stage of surface wave testing, inversion, involves finding one or more layered earth models whose theoretical dispersion curves match the experimental data. These trial models consist of stacked horizontal layers of infinite lateral extent whose thickness, mass density, and velocity (shear-wave velocity, V_S, being of primary interest) are constrained by the parameterization chosen prior to inversion. The inverse problem is inherently

[1]Ph.D. Candidate, Dept. of Civil, Architectural, and Environmental Engineering, Univ. of Texas at Austin, Austin, TX 78712 (corresponding author). ORCID: https://orcid.org/0000-0003-2857-3591. Email: yustm@utexas.edu

[2]Professor, Dept. of Civil and Environmental Engineering, Utah State Univ., Logan, UT 84322.

Note. This manuscript was submitted on March 18, 2022; approved on September 9, 2022; published online on November 22, 2022. Discussion period open until April 22, 2023; separate discussions must be submitted for individual papers. This paper is part of the ***Journal of Geotechnical and Geoenvironmental Engineering***, © ASCE, ISSN 1090-0241.

ill-posed, nonlinear, and mix-determined, with no unique solution (Vantassel and Cox 2021b; Foti et al. 2015). In many cases, this results in a very large number of velocity models fitting the experimental dispersion data and the data's associated uncertainty.

The nonuniqueness issue associated with surface wave inversion is compounded by the need to consider multiple trial model parameterizations with different numbers of layers as a means for investigating epistemic uncertainty when attempting to fit the experimental dispersion data (Vantassel and Cox 2021b; Cox and Teague 2016; Di Giulio et al. 2012). This is especially important when a priori information either is not available or does not extend to great enough depths to constrain the inversions. These trial parameterizations are used to vary the number of potential layers present in the subsurface models and set the acceptable search ranges for depths to boundaries and stiffness of each layer. The inversion results are highly affected by the parameterizations, and performing high-quality inversions requires analysts to use different parameterization options to fully explore potential conditions at the site and characterize the epistemic uncertainty of the inversion process. While this practice allows for a robust analysis of the experimental dispersion data and the associated uncertainty, it also generates many potential subsurface models for the site, which can present a challenge for engineers deciding which V_S profiles best represent the true subsurface layering for use in subsequent analysis and design. For this reason, analysts need a systematic and quantitative approach to evaluate all of these V_S profiles and determine which one(s) can most reasonably be expected to represent the true subsurface conditions at the site. While individual analysts should apply their engineering judgment and experience, it is important to investigate new approaches that enable more consistent performance of these evaluations across analysts so that engineers using the results can be confident in their quality.

This paper presents a new approach, called the DeltaVs method, for systematically evaluating the depths of layer boundaries across all acceptable models determined from several different inversion layering parameterizations as a means to identify significant subsurface layers from distinct clusters of layer boundaries. Using these clusters, the number and location of meaningful layer boundaries can be determined for many sites, even in the absence of a priori information, thereby allowing elimination of some parameterization options containing more, or fewer, boundaries and reduction in epistemic uncertainty. The distributions of layer boundaries within these clusters can then be used to determine statistics for the depths of layer boundaries that are consistent with the epistemic uncertainty of the models produced by the inversion procedure.

Here, the DeltaVs method is first explained and then demonstrated on 12 synthetic ground models published by Vantassel and Cox (2021b). The method's strengths and weaknesses are discussed in light of its performance in identifying significant layer boundaries and accurately characterizing the subsurface V_S associated with each synthetic model. Then it is applied to a field data set where its performance is evaluated relative to subsurface layering obtained from cone penetration test (CPT) data. As a good understanding of inversion uncertainty and nonuniqueness, particularly when caused by the choice of layering parameterization, is critical to applying DeltaVs, additional background information on the inversion phase of surface wave testing is discussed next.

Inversion Procedures

Before an inversion can begin, a target needs to be created that includes all the experimental dispersion data to be inverted. The analyst must determine which Rayleigh and/or Love mode(s) may have contributed to the dispersion data. This decision relies on the experience and judgment of the analyst to select a reasonable interpretation, and it can have a significant impact on the results of any subsequent inversions (Yust et al. 2018). Once the inversion target has been established, the first step associated with inverting surface wave dispersion data is developing a trial subsurface model, which is composed of a certain number of layers, each assigned a thickness (h), mass density (ρ), V_S, and compression wave velocity (V_P) or Poisson's ratio (ν). The second step is to obtain a theoretical dispersion curve for the trial model by solving the forward problem, for which the Thomson-Haskell transfer matrix (Thomson 1950; Haskell 1953) is the most common approach. The relationships between individual model parameters, such as layer thickness and velocity, and the resulting dispersion curve are complex and interconnected. Different combinations of parameters (e.g., a stiff, thin layer or a soft, thick layer) may have similar effects on the theoretical dispersion curve, which contributes to inversion nonuniqueness. The third step is to calculate the level of agreement (i.e., misfit) between the theoretical and experimental dispersion data as a means to judge the goodness of the trial model. The three steps are repeated iteratively, changing the trial model within the bounds of the parameterization for each iteration, in an attempt to increase agreement (i.e., minimize misfit) between the theoretical and experimental dispersion data.

While numerous misfit functions have been used for inversion optimization, they are generally in the form of an L2 norm of residuals, or a normalized version of such (e.g., root-mean square error). For example, the misfit equation proposed by Wathelet et al. (2004), as implemented in the Dinver inversion module of the popular open-source Geopsy software package (Wathelet et al. 2020), functions as a root-mean square error normalized by the dispersion uncertainty at each frequency. Consequently, the misfit value represents the difference, in terms of the number of standard deviations, between the theoretical dispersion curve and the mean values of the experimental dispersion data. A value of 1.0 indicates that, on average, across all points in the experimental dispersion data, the theoretical curve is one standard deviation away from the mean. Generally, misfit values below 1.0 are considered reasonable, with values below 0.5 indicating very good agreement between the theoretical curve and the mean trend of the experimental data, and values below 0.2 indicating exceptional agreement, which can be difficult to achieve with dispersion data collected at geologically complex sites (Yust 2018).

The search/optimization algorithms used to perform the trial model iterations generally fall into two categories: local search and global search. Local search algorithms only search the parameter space near the initial trial model and generally use linear optimization methods, such as least-squares regression (Nocedal and Wright 2006), to determine the single lowest-misfit (i.e., "best") model. These algorithms can be successful in providing a single velocity model that acceptably fits the experimental data, but the results are substantially influenced by the choice of the initial trial model and are highly susceptible to problems associated with local minima convergence (Socco et al. 2010). Additionally, the inherently convergent nature of the local search algorithm means that the results may fit the average trends in the experimental data but likely will not significantly represent the data's uncertainty.

Despite these limitations, and because of their relatively low computational requirements, local search algorithms still find use in practice, particularly for applications where large numbers of data sets are being inverted. Two prominent examples of these cases are the reports by Yong et al. (2013) and Kayen et al. (2013), which characterized 191 and 301 sites, respectively, using local search methods to invert surface wave data. Nonetheless, it is

difficult to propagate dispersion uncertainty into estimates of V_S uncertainty using local search methods. Thus, when estimates of V_S uncertainty are desired, global search methods are typically employed (e.g., Lai et al. 2005; Foti et al. 2009; Teague et al. 2018; Yust et al. 2018; Vantassel and Cox 2021b).

Global search algorithms include a wide variety of methods, including Monte Carlo, importance sampling, and genetic algorithms (Socco and Boiero 2008; Sambridge 1999a, b; Yamanaka and Ishida 1996). Other advancements in global search methods include the adaptive simulated annealing technique developed by Pei et al. (2007) and the joint analysis of Rayleigh-wave particle motion data presented by Dal Moro et al. (2018). These algorithms explore the entirety of the parameter space, repeatedly varying all model parameters within their prescribed bounds to find suites of the lowest-misfit models, making them much more computationally intensive than local search methods. The size of the parameter space can significantly affect the results from a global search algorithm (Socco et al. 2010; Di Giulio et al. 2012), so the parameter space must be broad enough to contain all reasonable results, while being sufficiently constrained to avoid wasting resources by investigating unreasonable models.

Model Parameterization

When a priori information like borehole lithology logs is available, the inversion parameter space should be constrained based on that information in order to reduce epistemic uncertainty and provide results that are most representative of true subsurface conditions. For example, if the depths to one or more significant impedance contrasts are known, the parameter space can be fixed such that layer boundaries occur at those depths (e.g., Teague et al. 2018). If no such information is available, particularly for layer boundaries that are deeper than existing boreholes, the analyst may be able to use supporting data, like fundamental frequency from H/V measurements (Thabet 2019; Yust et al. 2018; Fairchild et al. 2013) or regional velocity models (Shaw et al. 2015; Ramírez-Guzmán et al. 2012; Pratt and Schleicher 2021), to constrain depths to significant impedance contrasts. However, when a priori information either is not available or does not extend to great enough depths to constrain the inversions, true inversion uncertainty cannot be captured without considering multiple layering parameterizations.

As noted previously, the parameter space defines the number of layers within the velocity model as well as the properties of those layers (h, ρ, V_S, V_P). Each parameter must be either fixed or assigned a bounded range of acceptable values. Generally, when establishing parameterizations, the greatest emphasis is put on the number of layers, their thicknesses, and V_S, as these parameters most strongly effect the theoretical dispersion curve. Unfortunately, it is common for analysts to simply use a single layering parameterization when inverting surface wave data. For example, analysts will set up the inversion parameterization using a large number of thin layers with uniform thickness that are intended to allow the inversion to accurately resolve thin layers and anomalies. This practice is inconsistent with the decreasing ability to resolve thin layers as depth increases due to the vertical averaging inherent in surface wave propagation (Park et al. 1999), and can result in a significantly overparameterized model and poor results from the search algorithm (Socco et al. 2010; Crocker et al. 2021).

While the overparameterized model with many layer boundaries can be easily manipulated to fit the experimental data, inverted velocity models may not accurately reflect true subsurface conditions. For example, a site with sharp velocity contrasts, when inverted with too many layers, is likely to spread contrasts over several thinner layers, resulting in a more gradual change in velocity over a larger depth range. The opposite is also possible, where a site with gradual changes in velocity is overly simplified, resulting in high impedance contrasts being placed where they are not present. Literature has shown that the presence of high impedance contrasts can have a significant impact on site response (Baise et al. 2016) and that too many or too few layers can cause under- or overprediction of site response, particularly at high frequencies (Shible et al. 2018; Kaklamanos and Bradley 2018). Thus, accurately capturing the true subsurface layering is important.

Several studies have looked at the effects of using multiple layering parameterizations to investigate uncertainty and nonuniqueness associated with surface wave inversions. Di Giulio et al. (2012) inverted data sets from 14 European strong-motion stations using four distinct layering parameterizations and then ranked the results using the Akaike criterion to determine the most appropriate parameterization when considering misfit and model complexity. Hollender et al. (2018) characterized 33 French accelerometer stations with multiple layering parameterizations before utilizing available a priori information to eliminate results from some that were incompatible with known subsurface conditions from invasive testing, such as depth to bedrock or the presence of a low-velocity layer. Cox and Teague (2016) developed the layering ratio (LR) approach to systematically consider multiple layering parameterizations during inversion as a means to rigorously investigate epistemic uncertainty in the resulting V_S profiles. More recently, Vantassel and Cox (2021b) developed a new inversion parameterization approach called layering by number (LN), which they showed in many cases slightly outperforms LR. As LN inversion parameterization is used in the present study, it is described in greater detail next.

The LN approach requires the analyst to select a total number of layers (i.e., an LN value) for each inversion parameterization considered. Several LN values should be used as a means to investigate epistemic uncertainty in the inversion results. For shallow profiling (e.g., $d \leq 30$ m), LN values of 3, 5, or 7 may be appropriate, while for deeper profiling (e.g., $d \geq 30$ m) values of 10, 15, or 20 may be required. Regardless of the number of layers considered for a given LN parameterization, the minimum thickness ($h_{\min}$) of each layer is controlled by the minimum resolved wavelength, $\lambda_{\min}$, and set to $\lambda_{\min}/3$, while the maximum bottom depth is controlled by the maximum resolved wavelength, $\lambda_{\max}$, and set to a value chosen by the analyst, ranging from $\lambda_{\max}/3$ to $\lambda_{\max}/2$ (often referred to as the resolution depth, d_{res}), consistent with the resolution capabilities of the experimental dispersion data (Garofalo et al. 2016b). Both $\lambda_{\min}$ and $\lambda_{\max}$ depend on the array geometry (i.e., array length and sensor spacing) and the frequency content of the source. The minimum bottom depth for each layer is constrained by the bottom of the layer above it plus the minimum thickness value. If some a priori information is known, the depth and/or velocity values of some layers can be fixed while the remaining unfixed layers are free to vary according to the general constraints of the parameterization. The LN approach allows the inversion algorithm the freedom to distribute the layer boundaries in many different ways throughout the various trial models as the best possible solutions are sought. This freedom allows the LN approach to produce reasonable parameterizations for a wide variety of site conditions.

Profile Selection

While systematically exploring different parameterizations helps analysts investigate the epistemic uncertainty of inversion results, it does not change the fact that global search methods produce a large number of nonunique velocity models to be considered

for any given parameterization. This is particularly true when implementing uncertainty-consistent inversions, as recently developed by Vantassel and Cox (2021a), wherein at least 250 V_S profiles were required for each parameterization to appropriately replicate the uncertainty contained in the experimental dispersion data. The uncertainty in the final suite of inversion results can be broken down into two categories: intra- and interparameterization uncertainty. Intraparameterization uncertainty is due to the nonuniqueness of the global search inversion process as well as the uncertainty of the experimental data, and results in the variation of V_S profiles produced by a single parameterization. Interparameterization uncertainty arises from the need to consider multiple layering parameterizations, as the analyst often has no way of knowing which one is "correct" or most reasonable.

An example of interparameterization uncertainty is illustrated by the surface wave inversion results presented in Fig. 1, where the theoretical dispersion curves and V_S profiles resulting from three LN inversion parameterizations are shown. Specifically, the fundamental Rayleigh mode (R0) experimental dispersion data (generated using a synthetic ground model) and its uncertainty are plotted in terms of phase velocity versus wavelength in Fig. 1(a). Note that the dispersion uncertainty has been set equal to a 5% coefficient of variation (COV) for this synthetic example to be consistent with experimental dispersion uncertainties from several blind studies (Garofalo et al. 2016a; Cox et al. 2014). The data were inverted using Dinver, which utilizes a global importance sampling algorithm known as the neighborhood algorithm (Sambridge 1999a, b; Wathelet et al. 2005; Wathelet 2008), to find suites of models that fit the experimental dispersion data equally well when considering data uncertainty. Three options for subsurface layering parameterization are shown, ranging from models with 4 layers (LN = 4) to models with 14 layers (LN = 14). The 100 "best" (i.e., lowest-misfit) models for each layering parameterization are illustrated in terms of V_S in Fig. 1(b). While all 100 theoretical dispersion curves from each of these LN parameterizations fit the experimental dispersion data well, with misfit values ranging from 0.06 to 0.32 (note that the range of misfit values for each parameterization is provided in the figure legend in brackets), there is significant scatter in the V_S profiles and uncertainty regarding the true subsurface stiffness and layering. The single "best" model for each parameterization is shown in Fig. 1(c). The profiles shown in Figs. 1(b and c) demonstrate both intra- and interparameterization uncertainty. Intraparameterization uncertainty is shown by the variation among profiles from the same parameterization. For example, LN = 7 profiles have velocities ranging from roughly 500 to 1,000 m/s at a depth of 45 m. Interparameterization uncertainty of the results is shown by the variation in overall behavior and trends in each set of V_S profiles, such as where significant layer boundaries occur. For example, if the LN = 4 results are believed, a significant layer boundary occurs at about 23 m. However, if the LN = 7 results are believed, a significant layer boundary occurs at about 26 m, and if the LN = 14 results are believed, the impedance contrasts are more moderate, with several less abrupt layer boundaries spread between 20 and 30 m.

If a priori information is available, it can be used to eliminate parameterizations inconsistent with known site conditions, such as in Hollender et al.'s (2018) study noted previously, which subsequently reduces interparameterization uncertainty. However, when sufficient a priori information is not available, one must either retain all results and carry them forward into subsequent analyses (at the expense of significant epistemic uncertainty) or somehow determine a smaller number of profiles that best represent subsurface conditions. While the simple option of selecting only the single lowest-misfit profile across all parameterizations [e.g., the LN = 4 best profile with misfit = 0.06, as shown in Fig. 1(c)] has been used by some, this approach does not allow consideration of any intra- or interparameterization uncertainty. Another option is to calculate and retain statistical median V_S profiles from the results

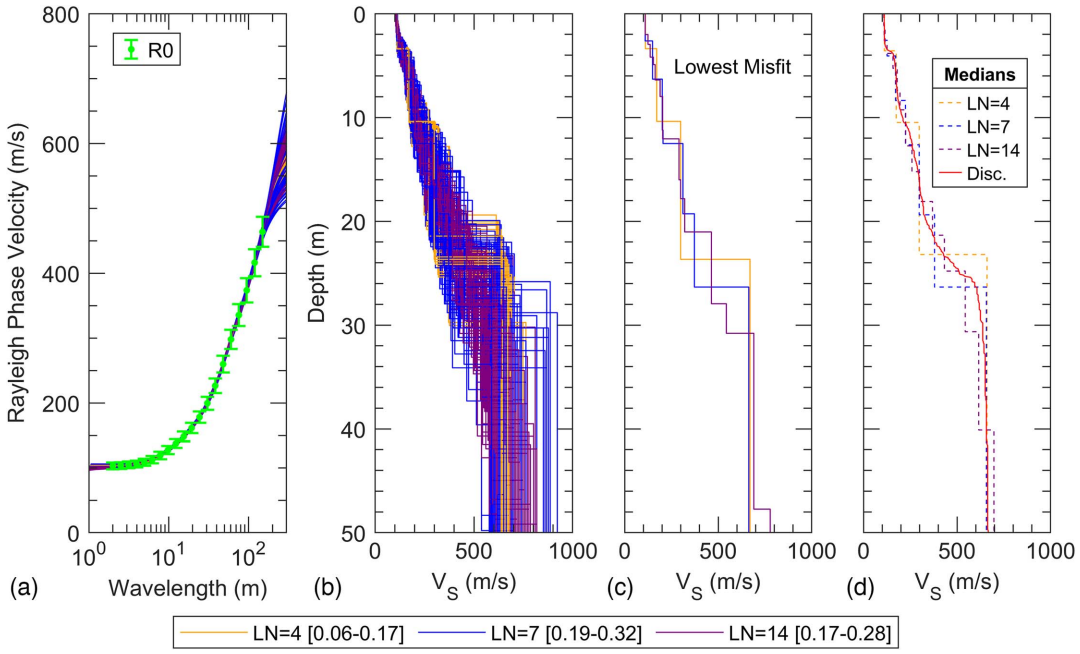

Fig. 1. Example inversion results for synthetic ground Model L: (a) the synthetic R0 experimental dispersion data and inversion-derived theoretical dispersion curves for the 100 lowest-misfit trial models from each LN parameterization (300 models total); the range of misfit values for the 100 best models from each parameterization is shown in brackets in legend; (b) the 300 inversion-derived V_S profiles; (c) the single lowest-misfit profile for each LN parameterization; the corresponding dispersion misfits are 0.06, 0.19, and 0.17 for LN = 4, LN = 7, and LN = 14 parameterizations, respectively; and (d) the median V_S profiles for each LN parameterization and discretized median V_S profile across all 300 profiles shown in (b).

J. Geotech. Geoenviron. Eng., 2023, 149(2): 04022126

for each parameterization, as illustrated in Fig. 1(d) with medians produced for the 100 best profiles from each parameterization. While this option allows for some consideration of both intra- and intermethod uncertainty and results in a manageable number of profiles, it does not help one determine which layering scenario(s) is most appropriate. A third option is to generate a single, discretized median profile calculated from the selected results of all parameterizations. Since each parameterization contains different numbers of layers, the profiles from all parameterizations must first be discretized into common, smaller depth intervals prior to calculating a median. The discretized median derived from the 300 selected profiles (the 100 best from each parameterization) is shown in Fig. 1(d). This approach does account for both inter and intra-parameterization uncertainty, but discretized median V_S profiles tend to smooth layer boundaries, as shown in Fig. 1(d), by mixing results from different parameterizations, some of which may not represent true subsurface layering. The discretized median approach is improved if interparameterization epistemic uncertainty can be reduced by using results only from parameterizations that best represent the true layering. This was the initial motivation for developing the DeltaVs method.

DeltaVs Procedure

The DeltaVs method seeks to estimate the number and depth of meaningful layer boundaries beneath a site from a large number of trial velocity models produced using global search inversions with multiple layering parameterizations. This is accomplished by identifying distinct clusters of layer boundaries within the large population of V_S profiles that fit the experimental dispersion data. Using these clusters, the number of meaningful layers can be determined for many sites, thereby allowing some parameterization options to be eliminated and epistemic uncertainty to be reduced. The distribution of layer boundaries within these clusters can then be used to determine statistics for the depths of layer boundaries that are consistent with the epistemic uncertainty of the models produced by the inversion procedure. To illustrate the steps of the DeltaVs procedure, its steps are first demonstrated on a synthetic ground model, denoted F, one of the 12 synthetic ground models from Vantassel and Cox (2021b) used to develop an inversion workflow called SWinvert, which uses the Dinver module of the opensource software Geopsy (Wathelet et al. 2020) as an inversion engine. Results obtained from applying the DeltaVs method to the rest of the 12 synthetic ground models are discussed further subsequently.

Model F is identified by Vantassel and Cox (2021b) as a low-variance data set that can be inverted with reasonable accuracy. While it is one of the lower-complexity models the researchers studied, it is by no means the least complex in the suite and serves as a good example to illustrate the DeltaVs method. Model F has three layers (Fig. 2): a surface layer with H = 4 m and V_S = 100 m/s, an intermediate layer with H = 10 m and V_S = 200 m/s, and a half-space with V_S = 400 m/s. The synthetic experimental dispersion data and 600 inversion-derived theoretical dispersion curves for Model F are shown in Fig. 2(a). All 600 of the theoretical dispersion curves (the best 100 from six LN parameterizations) fit the synthetic experimental data well, with misfit values ranging 0.02–0.39, falling well within the 5% COV error bars. While the inverted velocity profiles [Fig. 2(b)] follow a relatively consistent trend across the various LN parameterizations, the parameterizations with fewer layers indicate abrupt velocity contrasts while those with more layers tend to smooth out the contrasts. The median profiles from each LN parameterization are shown in Fig. 2(d) and display the same general behavior as the individual inverted profiles. Without the overlain true V_S profile, pinpointing the exact locations of the layer boundaries is

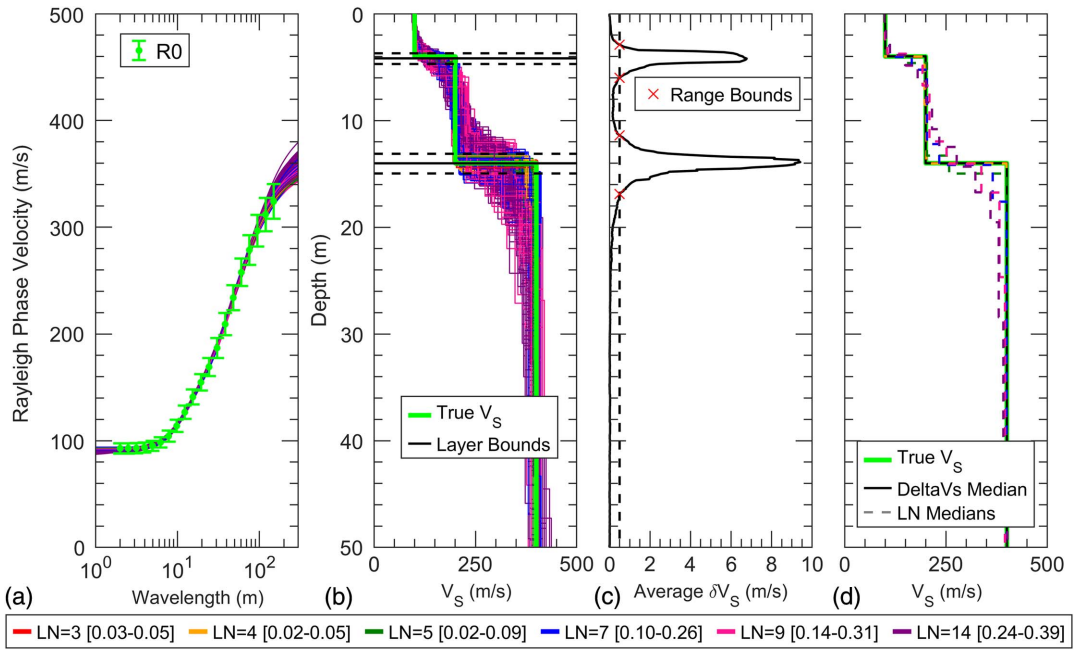

Fig. 2. Summary of inversion results for synthetic ground Model F: (a) the synthetic R0 experimental dispersion data and inversion-derived theoretical dispersion curves for the 100 lowest-misfit trial models for each LN parameterization (600 models total); the range of misfit values is shown in brackets in legend; (b) the 600 inversion-derived V_S profiles shown with the true V_S profile and lognormal median $\pm\sigma_{\ln}$ of statistical layer boundaries identified by the DeltaVs method; (c) the average change in $\delta V_{S,\text{avg}}$ with depth and the depth ranges used to determine layer boundaries shown in (b); and (d) the median V_S profiles for each LN parameterization, true V_S profile, and the DeltaVs median profile derived from 100 lowest-misfit trial models from parameterization developed from the DeltaVs results.

J. Geotech. Geoenviron. Eng., 2023, 149(2): 04022126

challenging and uncertain using either the hundreds of inverted V_S profiles or their respective medians.

The DeltaVs method provides analysts with a tool for locating significant layer boundaries in a systematic way that is not dependent on having a priori information. First, the V_S profiles from the different LN parameterization inversions need to be standardized in terms of depth discretization. This is accomplished in Step 1, by discretizing all of the V_S profiles at common depth intervals and to a common maximum depth. The depth discretization interval (d_{disc}) should be selected such that it is small enough to retain sufficient accuracy in the locations of layer boundaries but large enough to prevent an excessive number of data points. Generally, the depth discretization interval can be set at 0.1 m, as it was here for Model F. The maximum discretization depth should be set to d_{res} as determined from the experimental data used for the inversions. For Model F, d_{res} was set to a value of $\lambda_{\max}/3 = 50$ m.

Once the velocity models have all been discretized, the DeltaVs method proceeds to Step 2, calculating the change in velocity (δV_S) between every pair of successive discretized points within each velocity model. This results in δV_S profiles that have one fewer sample than the original depth-discretized V_S profiles, and corresponding depths located halfway between the original depths of the discretized profiles (e.g., the sample corresponding to the change in velocity from 10 m to 10.1 m is located at a depth of 10.05 m). Next, in Step 3, the δV_S profiles are averaged together at each common depth to get a single profile that represents the average change in velocity with depth across all trial models and all parameterizations. This profile is then, in Step 4, smoothed using an arithmetic moving average, with the number of samples (n) equal to $h_{\min}/d_{disc}$ rounded up to the nearest whole number. For Model F, with $h_{\min} = \lambda_{\min}/3 = 0.67$ m and $d_{disc} = 0.1$ m, seven samples were used to smooth the arithmetic mean. The resulting smoothed $\delta V_{S,\text{avg}}$ profile for Model F is shown in Fig. 2(c). This $\delta V_{S,\text{avg}}$ profile is then used in Step 5 to identify depth ranges over which significant velocity changes occur.

When a wide variety of layering options are used for inversion parameterizations, it is often relatively simple to identify parameterizations that do not have a large enough number of layers to properly characterize the site, as the inversions results have relatively high misfit values compared with other parameterizations. However, when more than enough layers are present in a parameterization, the search algorithm can easily fit the experimental data by effectively merging several thinner layers with similar velocities. As such, depth ranges where there are high $\delta V_{S,\text{avg}}$ should be selected such that they are likely to contain all parts of a potential real layer boundary that may have been split across multiple layers. For example, for Model F, two distinct depth ranges of high $\delta V_{S,\text{avg}}$ are easily identifiable as spikes/peaks [Fig. 2(c)]. The bounds of each depth range are denoted by red ×'s where the $\delta V_{S,\text{avg}}$ profile crosses a threshold of 0.5, marked by a vertical dashed line. In the course of this work, several values for this threshold were investigated, and it was found that 0.5 worked well for identifying the bounds of each meaningful depth range. Peaks are considered to be the range of depths between which the $\delta V_{S,\text{avg}}$ values exceed 0.5, with one significant maxima in between. Again, referring to Fig. 2(c), the depth range bounds for the two potential layer boundaries are 2.85–5.96 m for the first layer and 11.35–16.85 m for the second layer. While not the case for Model F, if the $\delta V_{S,\text{avg}}$ profile does not fall below the 0.5 threshold between two significant maxima, the depth corresponding to the local minima should be used as the ending value for the first distribution and the starting value for the second. This can occur when layer boundaries are close to one another. Furthermore, if the $\delta V_{S,\text{avg}}$ profile exceeds the threshold for an extended range of depths, the analyst must use judgment to assess whether any maxima within that range represent a distinct peak for which a depth range can be bounded. More complex examples illustrating these points are provided next.

Once the upper and lower depth range bounds have been identified, the individual discretized δV_S profiles are used in Step 6 to develop a list for each depth range that characterizes the locations and magnitudes of the velocity changes for all layer boundaries within that range. For each layer boundary in each δV_S profile, the corresponding depth is added to the list multiple times proportional to the magnitude of the velocity change across the layer (e.g., a velocity change of 5 m/s at a depth of 10 m results in the value 10 being added to the list five times), which favors the importance of stronger velocity contrasts or depths at which a greater number of contrasts occur. These two factors, the number and magnitude of velocity contrasts, are coupled within the δV_S profile. This weighting results in a long list of layer depths where the number of times an individual depth appears in the list is directly proportional to the total magnitude of all velocity changes at that depth. The weighting applied here is also consistent with the assumption made in the LN parameterization scheme that velocity changes occur at discrete depths within the V_S profile. Analysts may wish to adjust the weighting depending on the expected behavior at their site (e.g., gradual transitions in velocity). In Step 7, each list of layer boundary depths is transformed into log space and, in Step 8, the mean and standard deviation values for each layer boundary are calculated assuming a normal distribution. In Step 9 these values are transformed back into linear space as the lognormal medians and standard deviations ($\sigma_{\ln}$) of the layer boundaries. The two statistical layer boundaries identified and characterized using this process for Model F are shown in Fig. 2(b) with their medians and $\pm 1\sigma_{\ln}$. The first statistical layer boundary has a lognormal median and a standard deviation of 4.17 m and 0.12, respectively. The second statistical layer boundary has a lognormal median and a standard deviation of 14.01 m and 0.07, respectively. Both boundaries are in very good agreement with the layer depths from the true V_S profile, which occur at 4 and 14 m, respectively.

If an analyst were to simply select the single best trial model across all parameterizations with the lowest misfit, the resulting trial model would be a 4-layer profile (LN = 4) with a misfit value of 0.02 and layer boundaries at depths of 3.92, 4.59, and 13.97 m. Or, if by some a priori information the analyst knew that the correct number of layers for Model F was three, the resulting lowest-misfit trial model from the LN = 3 parameterization could be used to estimate layer boundaries. For this case, that model would have a misfit value of 0.03 and layer boundaries at 4.00 and 13.85 m. While both of these approaches to determining the most likely layer boundaries would be quite accurate, neither approach would allow for a rigorous consideration of uncertainty in a real-world application where the true subsurface V_S profile is unknown. Furthermore, without a priori information regarding the anticipated layering beneath the site, one would struggle to justify choosing only one or two most likely trial models, particularly since the misfit values for all parameterizations are very low.

On the other hand, the DeltaVs method utilizes all inversion results and still provides accurate layer boundaries with estimates of uncertainty. Indeed, if desired, the layer boundaries from the DeltaVs method can be used subsequently to justify considering only those models/parameterizations that yield layer boundaries similar to the ones obtained from the DeltaVs method (e.g., LN = 3 and LN = 4). Finally, as a means to illustrate the DeltaVs method's robustness, even if the inversion results from the LN = 3 parameterization are removed from consideration in the present example, and only the V_S profiles from the LN = 4, 5, 7, 9, and 14 parameterizations are included, the lognormal median and standard deviation

for the first boundary changes minimally to 4.20 m and 0.13, respectively, while the statistics for the lower boundary stay the same. This demonstrates that the boundary locations identified via the DeltaVs method have not been significantly biased by a large number of the convergent LN = 3 velocity profiles that closely match the true V_S profile, which also has exactly three layers. This also shows that the DeltaVs method can determine the correct number of layer boundaries even if that number had not been explicitly considered in the initial set of inversion layering parameterizations.

As can be observed, the DeltaVs method accurately identified the two distinct layer boundaries in the true Model F. These results correctly indicate that the true subsurface model is composed of three distinct layers, with layer boundaries most probably located within the calculated statistical ranges. These results can be used in several ways to reduce the epistemic uncertainty in the inverted V_S profiles. One option is to simply choose the inversion parameterization that most closely represents the layering determined from the DeltaVs procedure. In this case, it is LN = 3, which contains two distinct layer boundaries. Or the locations of the DeltaVs layer boundaries can be used to inform a new inversion with more restricted layering parameterizations. To demonstrate this, a new three-layer parameterization was developed for Model F where the layer boundaries were constrained to depth ranges within $\pm 2\sigma_{\ln}$ of the identified median depths. Next, the lognormal median and standard deviation of all of the discretized V_S profiles from the original LN parameterizations were calculated for the regions between these depth ranges, and the velocity of each layer in the new parameterization was constrained to be within $\pm 2\sigma_{\ln}$ of the median velocity. The median profile from the resulting 100 lowest-misfit profiles of this new layering parameterization is shown as a solid black line in Fig. 2(d) and labeled in the legend "DeltaVs Median." In this case, the DeltaVs median very closely matches the true V_S profile. Similarly, the LN = 3 median V_S profile matches the true V_S profile quite well, suggesting that either approach is a reasonable way to reduce epistemic uncertainty. While the example in Fig. 2 shows that the DeltaVs method is promising, Model F also contains very distinct layer boundaries with large impedance contrasts. In order to judge if the DeltaVs method identifies layer boundaries for different subsurface conditions (e.g., deeper layers, more layers, layers with fewer impedance contrasts), more subsurface models must be investigated.

Synthetic Ground Model Examples

In order to rigorously evaluate the efficacy of the DeltaVs method, it has been applied to a suite of 12 synthetic ground models, one of which is Model F. These 12 ground models were developed by Vantassel and Cox (2021b) as part of the SWinvert inversion workflow and were designed to represent a broad range of subsurface conditions from simple to complex. The models are open-access and publicly available through the DesignSafe-Cyberinfrastructure (Vantassel and Cox 2020). The information available for each includes the true V_S profile (in fact, the entire subsurface ground model) and the synthetic experimental R0 dispersion data with uncertainty. The true V_S profile for each synthetic ground model is provided in Fig. 3. It will be noted that these profiles range from 1-layer models (left-hand column) to 7-layer models (right-hand column), with layer impedance contrasts that range from moderate [Figs. 3(a–e)] to strong [Figs. 3(i–l)]. The suite of models does not have any profiles that include velocity reversals, however. Subsurface models with velocity reversals are especially hard to invert and generally require a priori information to properly constrain their true thickness and stiffness. Otherwise, the search algorithm can simply combine very high and very low velocity layers of varying thickness in unrealistic ways to fit the experimental data. As the DeltaVs method has not been investigated relative to sites with velocity reversals, one should not apply it to cases where the dispersion data contain obvious signs of velocity reversals (e.g., dips or troughs in the dispersion data). For these cases, one may wish to consider the adaptive simulated annealing technique developed by Pei et al. (2007). However, caution must be exercised when applying any inversion algorithm for the purpose of resolving low-velocity layers without supporting information to better constrain the inversion results.

The dispersion data for each synthetic ground model consist of 20 log-wavelength samples ranging from wavelengths of 2 to 150 m with a COV of 5%. For the present work, this dispersion data were converted from wavelength velocity to frequency slowness in preparation for inversions using the Dinver module of Geopsy. A total of six LN parameterizations were used to invert the synthetic ground models with layer quantities of 3, 4, 5, 7, 9, and 14. The parameterizations for all 12 synthetic ground models were set up with a minimum layer thickness of $\lambda_{\min}/3 = 0.67$ m and a maximum layer bottom depth of $\lambda_{\max}/3 = 50$ m. Mass density was assigned a constant value of $\rho = 2{,}000$ kg/m^3, allowing impedance contrasts to be expressed simply as the ratio of the layer's velocities (V_{i+1}/V_i). The inversions for all 12 synthetic ground models were performed in accordance with the SWinvert workflow using the Dinver tuning parameters recommended by Vantassel and Cox (2021b). Each inversion considered a total of 60,000 trial models, including 10,000 initial Monte Carlo models and 50,000 global search models spread across 250 iterations. These inversions each took about 1–2 min running on a moderately powerful desktop computer. As with the SWinvert recommendations, each inversion was performed 10 times to account for the variations that may result from the random starting seed of the neighborhood algorithm. Hence, 60 inversions were performed for each synthetic ground model (6 parameterizations with 10 random starting seeds), resulting in 3.6 million trial models searched (60 inversions each with 60,000 trial models). The 10 lowest-misfit velocity models from each of the 10 inversion trials performed for each layering parameterization were saved, yielding a total of 100 "best"/lowest-misfit subsurface models per parametrization. The application of the DeltaVs method to the inversion results from all 12 synthetic ground models is presented next.

Results for All Synthetic Ground Models

The layer boundaries identified for all 12 synthetic ground models are shown in Fig. 3, along with the true V_S profiles and the 100 lowest-misfit V_S profiles obtained from inversion using each of the six LN parameterizations (i.e., 600 total inverted V_S profiles). Across the 12 models evaluated, the DeltaVs method did a good, but not perfect, job of identifying significant layer boundaries present in the true ground models. As noted previously, the models in the upper left-hand corner are the least complex, with fewer layers and lesser impedance contrasts, while the models in the lower right-hand corner are more complex, with more layers and stronger impedance contrasts. The DeltaVs method accurately identified all layer boundaries in the two- and three-layer synthetic ground models [Figs. 3(a, b, e, f, i, and j)]. Across all six, the median layer depths identified using the DeltaVs method were within 5% of the true layer depths, with lognormal standard deviations ranging from 0.04 to 0.13. It must be noted that every median error greater than 2% occurred when the true depth of the layer boundary was less than 10 m. This is not indicative of poorer identification of shallow layers but rather is a statistical result of smaller

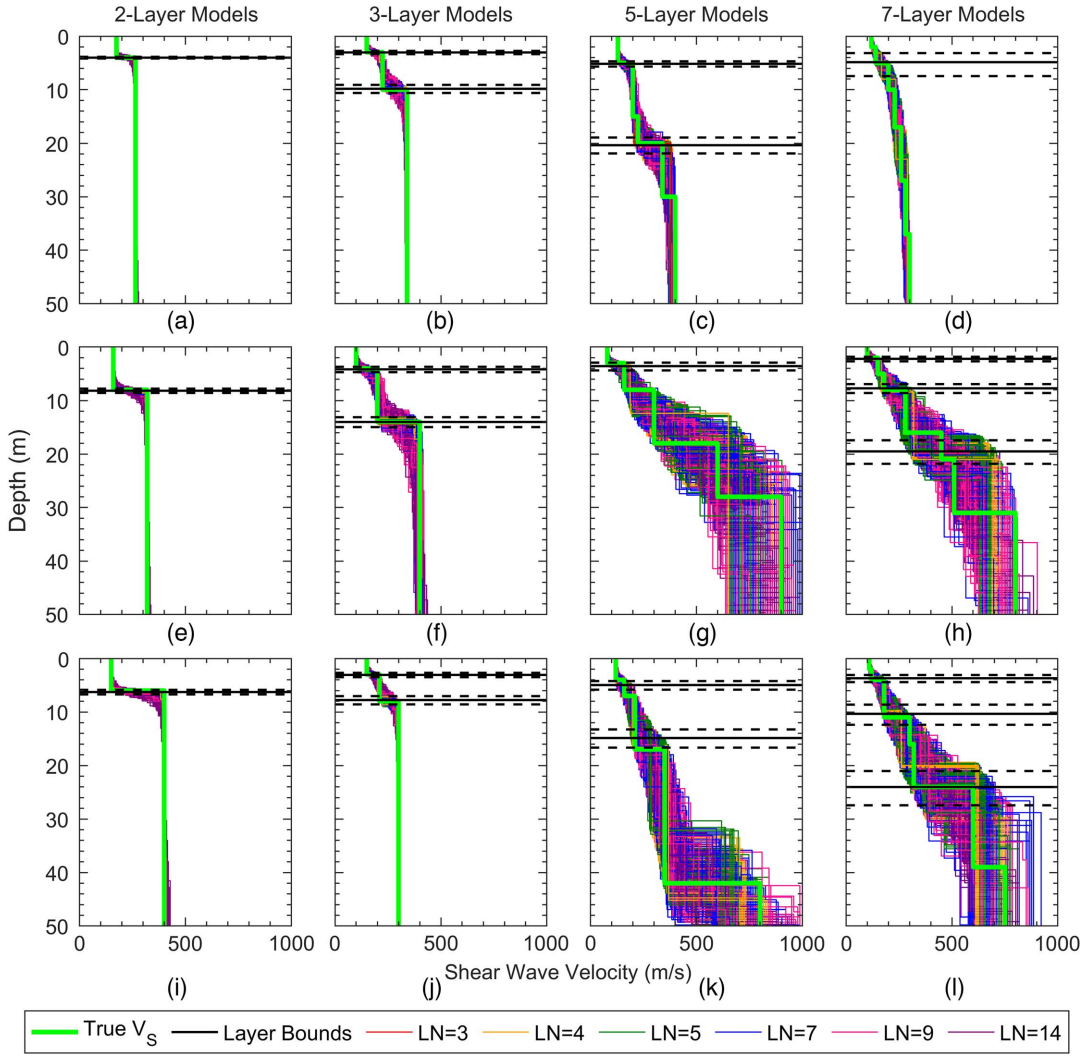

Fig. 3. Summary of inversion and layering results for all 12 synthetic ground models, including the true V_S profiles, inversion-derived V_S profiles for each LN parameterization, and lognormal median $\pm\sigma_{\ln}$ of statistical layer boundaries identified by the DeltaVs method for each synthetic model.

absolute errors having a larger relative impact at shallow depths (e.g., an absolute error of 0.2 m results in a much higher percentage error for a layer boundary at a depth of 3 m than one at a depth of 15 m). For the 6 synthetic ground models consisting of five or seven layers [Figs. 3(c, d, g, h, k, and l)], the results were less generalizable. For all of these models, with the exception of Model C, the results from the LN = 3 parameterization were rejected from consideration prior to applying the DeltaVs method, as it was not possible to acceptably fit the dispersion data and obtain low misfit values (≤1.0) when using only three layers. Results from 4 models [Figs. 3(c, g, h, and l)] are discussed in detail as a means to further illustrate the DeltaVs method's strengths and weaknesses.

Synthetic Ground Model C

Model C is a 5-layer model with layer boundaries at depths of 5, 15, 20, and 30 m. The impedance contrasts at two of these boundaries, 5 and 20 m, exceed 1.5, while the other two boundaries have impedance contrasts below 1.2. The inversion results for Model C are shown in Fig. 4, along with the true V_S profile and the statistical layer boundaries identified using the DeltaVs method. While the model has four layer boundaries, only two distinct peaks are easily identifiable in the δV_S profile, with depth ranges of 3.95–6.65 and 16.65–24.15 m, respectively. The first statistical layer boundary has a lognormal median and a standard deviation of 5.16 m and 0.09, respectively. The second statistical layer boundary has a lognormal median and a standard deviation of 20.37 m and 0.07, respectively. Both identified boundaries are in very good agreement (within 4%) with the actual high impedance contrast boundaries in the true V_S profile at 5 and 20 m. These results highlight that the DeltaVs method works best at identifying significant layer boundaries (those with high impedance contrasts). The low-contrast boundaries simply appear not to have enough impact on the curvature of the dispersion data to be resolved through the inversion process. This is reinforced by the fact that Model C is the only model with more than 3 layers for which the LN = 3 parameterization results were acceptable. LN = 3 was still able to fit the target dispersion data with misfit values less than 0.1, despite having two fewer layers than the true ground model. So the DeltaVs method accurately resolved the number and location of the significant layer boundaries, but it could not detect the weak impedance contrasts. A DeltaVs median profile was developed for this model using the same procedures outlined for Model F, with the new inversion parameterization constrained by the layer boundaries obtained from the DeltaVs results. As with Model F, this new DeltaVs-informed profile also closely matched the true V_S model

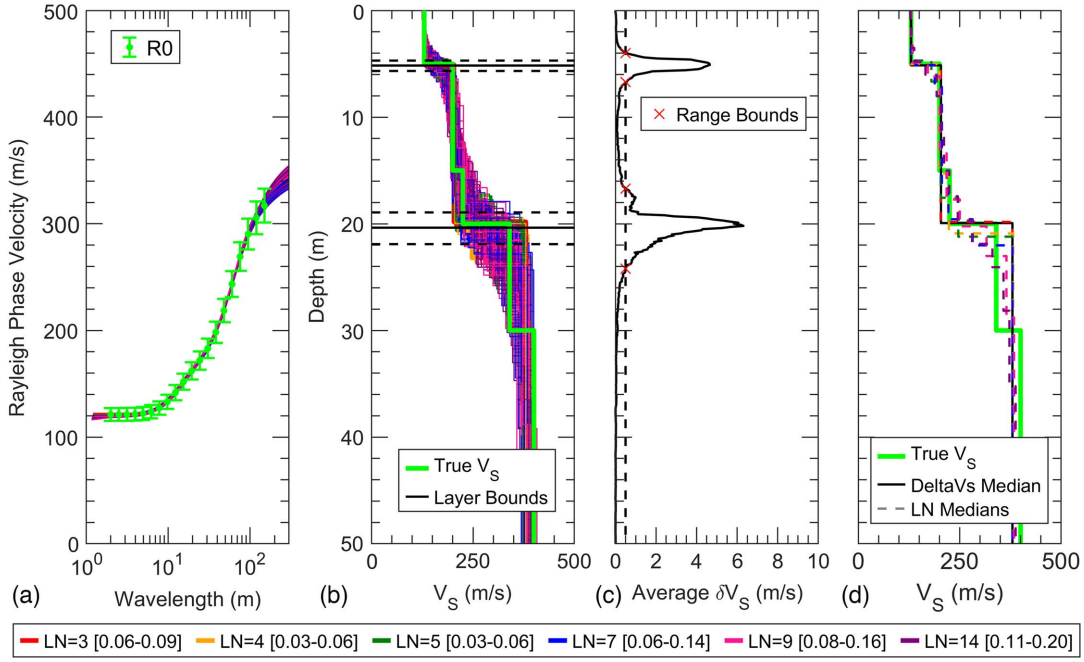

Fig. 4. Summary of inversion results for Model C: (a) the synthetic R0 experimental dispersion data and inversion-derived theoretical dispersion curves for the 100 lowest-misfit trial models from each LN parameterization (600 models total); the range of misfit values for 100 best models from each parameterization is shown in brackets in legend; (b) the 600 inversion-derived V_S profiles shown with the true V_S profile and lognormal median $\pm\sigma_{\ln}$ of statistical layer boundaries identified by the DeltaVs method; (c) the average change in $\delta V_{S,\text{avg}}$ with depth and the depth ranges used to determine layer boundaries shown in (b); and (d) the median V_S profiles for each LN parameterization, true V_S profile, and DeltaVs median profile derived from 100 lowest-misfit trial models from parameterization developed from the DeltaVs results.

[Fig. 4(d)]. However, the agreement in this case was not exact because only two of the four layer boundaries present in the true V_S model were identified.

Synthetic Ground Model G

Model G was explicitly identified by Vantassel and Cox (2021b) as a high-variance data set that was challenging to accurately resolve using surface wave inversions. It is a 5-layer model with boundaries at depths of 3, 8, 18, and 28 m. All four of these boundaries have impedance contrasts at or above 1.5. The inversion results for Model G are shown in Fig. 5, along with the true V_S profile and the identified layer boundaries. Despite having high impedance contrasts, only one distinct peak can be identified in the δV_S profile. The depth range for this peak extends from where the 0.5 threshold is crossed at 2.05 m down to the first local minima at 5.85 m. The δV_S profile does not fall below the 0.5 threshold at this minima, but does appear to briefly level off, providing a reasonable depth to end the range. Below this minima, the δV_S profile generally exceeds 2.0 for an extended range of depths, with no distinct individual peaks. The sole depth range identified produces a lognormal median and a standard deviation of 3.57 m and 0.20, respectively. This agrees somewhat with the location of the true layer boundary at 3 m; however, the median error of 19% and the standard deviation of 0.20 are higher than those for the accurately identified layer boundaries discussed thus far for other synthetic ground models. While the results from Model C suggest that impedance contrasts >1.5 can be located, the results from Model G seem to caution against drawing a broad conclusion from this observation. In fact, Model G's results suggest that not only does an impedance contrast need to be relatively high; it also needs to be relatively isolated to be easily identifiable using the DeltaVs method. When the large impedance contrasts are grouped too closely together, their influences on the dispersion data appear to smear together. The effect of this is visually displayed by the inversion V_S profiles in Fig. 5(b), which do not appear to have any coherent jumps or layer boundaries between the surface and the top of the half-space. As the DeltaVs method was not successful at identifying distinct layer boundaries, it is not possible to perform new inversions with refined layering parameterizations for Model G as a means to reduce epistemic uncertainty. Thus, when the DeltaVs method results in a δV_S profile that is similar to the one for Model G, analysts cannot accurately determine layer boundaries and have to accept greater epistemic uncertainty associated with the various LN parameterizations.

Synthetic Ground Model H

Model H is a 7-layer model with boundaries at 2, 5, 8, 16, 21, and 31 m. Like Model G, Model H was explicitly identified by Vantassel and Cox (2021b) as a high-variance data set that is challenging to accurately resolve using surface wave inversions. The boundaries at 2, 8, 16, and 31 m have impedance contrasts at or above 1.5, while the boundaries at 5 and 21 m have contrast at or below 1.2. The inversion results for Model H are shown in Fig. 6, along with the true V_S profile and the statistical layer boundaries identified by the DeltaVs method. Three distinct peaks can be identified in the δV_S profile, although local minima were used to bound the depth ranges where the value of δV_S visually leveled off without passing below the 0.5 threshold. The depth ranges identified are 1.05–3.45, 5.95–9.85, and 15.25–25.15 m. Despite being substantially broader than the first two, the third peak is still highly distinct from the δV_S values of the surrounding depths and cannot be ignored. The first statistical layer boundary has a lognormal median and a standard deviation of 2.21 m and 0.19, respectively. The second statistical layer boundary has a lognormal median and a standard deviation of 7.72 m and 0.11, respectively. The third statistical

J. Geotech. Geoenviron. Eng., 2023, 149(2): 04022126

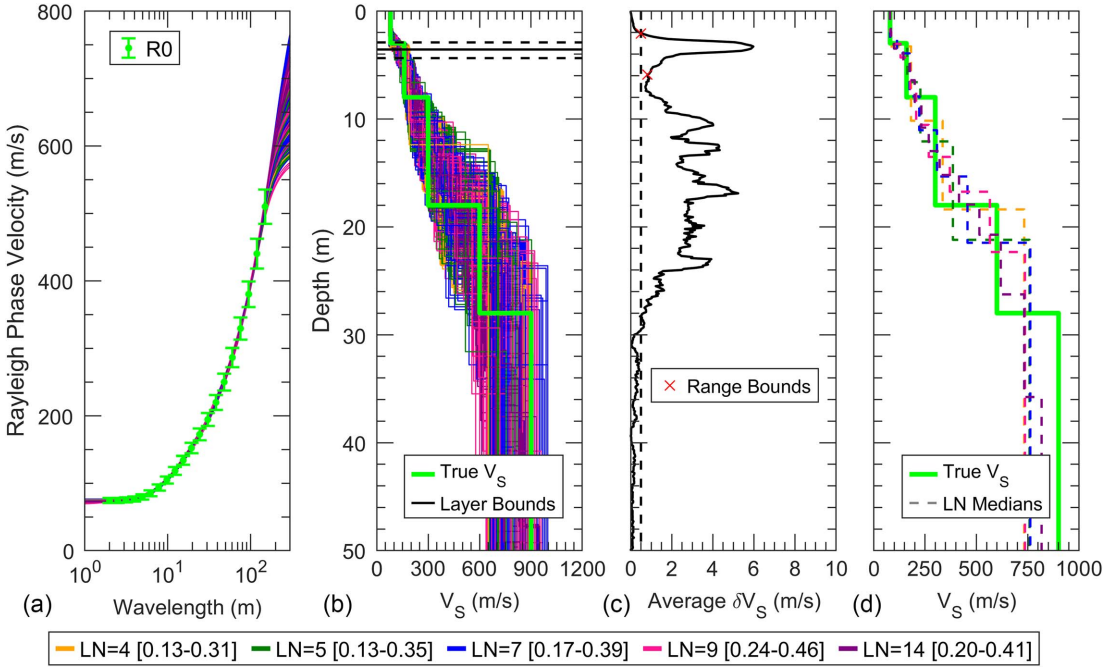

Fig. 5. Summary of inversion results for Model G: (a) the synthetic R0 experimental dispersion data and inversion-derived theoretical dispersion curves for the 100 lowest-misfit trial models from each LN parameterization (500 models total); the range of misfit values for the 100 best models from each parameterization is shown in brackets in legend; (b) the 500 inversion-derived V_S profiles shown with true V_S profile and lognormal median $\pm\sigma_{\ln}$ of statistical layer boundary identified by the DeltaVs method; (c) the average change in $\delta V_{S,\text{avg}}$ with depth and depth ranges used to determine layer boundary shown in (b); and (d) the median V_S profiles for each LN parameterization and true V_S profile.

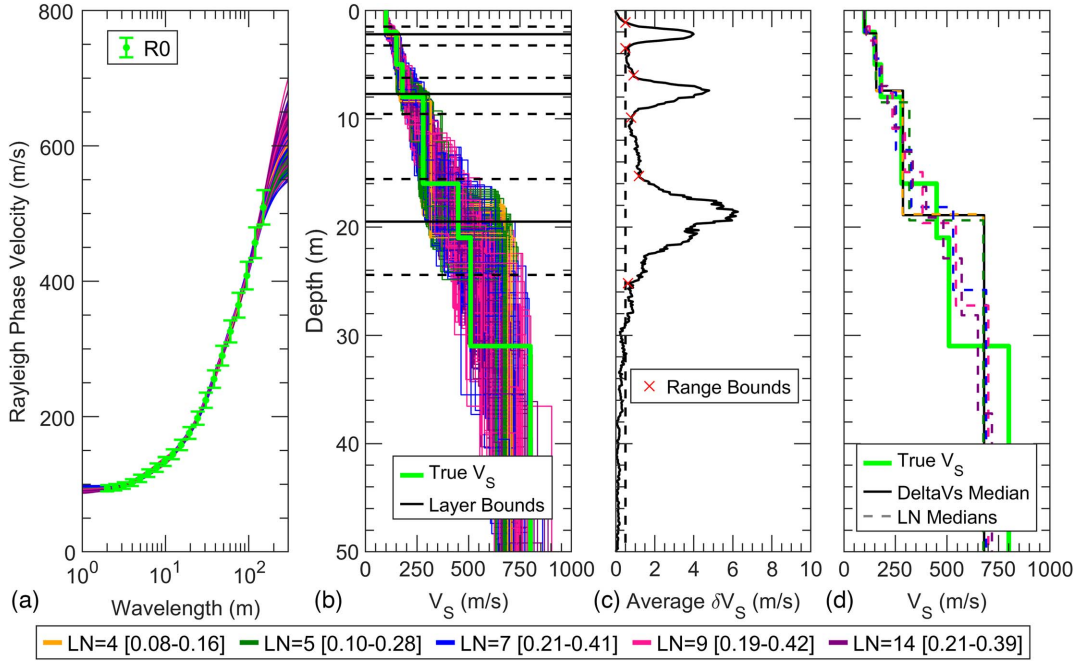

Fig. 6. Summary of inversion results for Model H: (a) the synthetic R0 experimental dispersion data and inversion-derived theoretical dispersion curves for the 100 lowest-misfit trial models from each LN parameterization (500 models total); the range of misfit values for the 100 best models from each parameterization is shown in brackets in legend; (b) the 500 inversion-derived V_S profiles shown with true V_S profile and lognormal median $\pm\sigma_{\ln}$ of statistical layer boundaries identified by the DeltaVs method; (c) the average change in $\delta V_{S,\text{avg}}$ with depth and depth ranges used to determine the layer boundaries shown in (b); and (d) the median V_S profiles for each LN parameterization, true V_S profile, and DeltaVs median profile derived from 100 lowest-misfit trial models from parameterization developed from the DeltaVs results.

layer boundary has a lognormal median and a standard deviation of 19.51 m and 0.11, respectively. The first and second statistical layer boundaries agree well with the high-contrast layer boundaries in the true V_S profile at 2 and 8 m, respectively. The third statistical layer boundary at 19.51 m does not agree particularly well with any of the true layer boundaries. Instead, it appears that this peak in δV_S values is caused by the combined effects of three layer boundaries in the true V_S profile between 16–31 m. Two of these layers at 16

J. Geotech. Geoenviron. Eng., 2023, 149(2): 04022126

and 31 m have large impedance contrasts, while the layer at 21 m has a smaller impedance contrast. The 19.51-m statistical layer boundary's proximity to the true layer boundary at 21 m appears to be coincidental. Thus, another important observation is made; that is, while a distinct peak may be present in the δV_S profile, it may not always correspond to a single, real layer boundary. This suggests that distinct yet broad peaks in the δV_S profile may indicate the presence of more than one layer boundary within or near the identified depth range of the peak. The DeltaVs median developed for this site using a new inversion with four layers is shown in Fig. 6(d). In this case, the new DeltaVs median V_S profile agrees well with the true V_S profile over the top 16 m. Below this depth, the DeltaVs profile performs no better than the other LN parameterizations.

Synthetic Ground Model L

Model L is a 7-layer model with boundaries at 2, 4, 11, 16, 24, and 39 m. The boundaries at 4, 11, and 24 m have impedance contrasts at or above 1.5, while the boundaries at 2, 16, and 39 m have contrasts at or below 1.25. The inversion results for Model L are shown in Fig. 7, along with the true V_S profile and the statistical layer boundaries identified by the DeltaVs method. Three distinct peaks can be identified in the δV_S profile, although the upper and lower peaks are much more distinct than the middle one. Using the 0.5 threshold and local minima, the depth ranges identified around these peaks are 2.25–5.65, 6.55–13.85, and 18.75–32.05 m. The first statistical layer boundary has a lognormal median and a standard deviation of 3.69 m and 0.18, respectively. The second statistical layer boundary has a lognormal median and a standard deviation of 10.34 m and 0.18, respectively. The third statistical layer boundary has a lognormal median and a standard deviation of 24.02 m and 0.13, respectively. All three statistical layer boundaries agree well with the high-contrast layer boundaries in the true V_S profile at 4, 11, and 24 m. While the first and second statistical layer boundaries have median errors of 8% and 6%, respectively, they still provide useful information about the number of significant layers and their approximate locations. The third statistical layer boundary agrees extremely well with the true layer boundary at 24 m. This accuracy is likely attributable to the high impedance contrast of the boundary (1.875) as well as the fact that no other significant impedance contrasts occur within 13 m above or 15 m below the boundary. Unlike the behavior observed with Model H, only one significant layer boundary is present in this depth range, despite the high standard deviation and broad peak of the δV_S profile. Overall, the results for Model L are similar to those for Model C and can be considered quite successful at resolving the locations of significant layer boundaries. The DeltaVs median profile developed for this site based on a new inversion is shown in Fig. 7(d). While this new median profile contains only three of the four layer boundaries present in the true V_S profile, it matches the profile quite well over the full depth range and in fact agrees with the true V_S profile better than any of the median V_S profiles from the initial LN parameterizations.

DeltaVs Application to Real Field Data

In order to test the efficacy of the DeltaVs method on real field data, it was applied to a surface wave data set collected at the Hornsby Bend test site in Austin, TX. The data were collected using a 94-m long MASW array consisting of 48, 4.5-Hz vertical geophones placed at 2-m spacings. Three sources were used: the NHERI@U-Texas T-Rex and Thumper mobile shakers (Stokoe et al. 2020) and

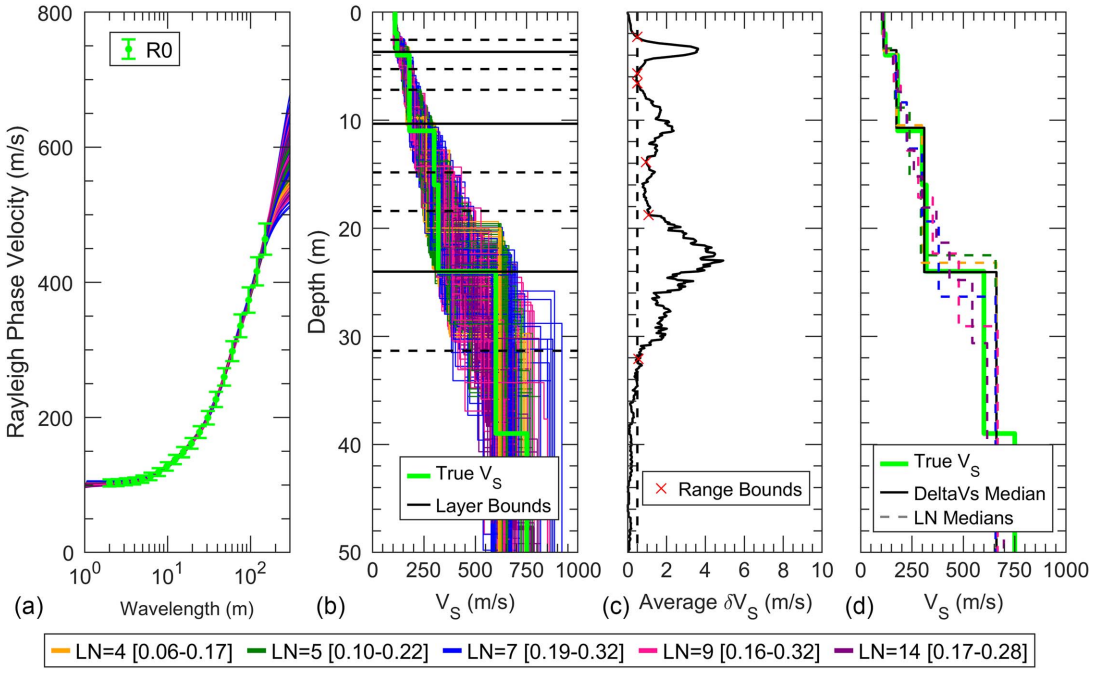

Fig. 7. Summary of inversion results for Model L: (a) the synthetic R0 experimental dispersion data and inversion-derived theoretical dispersion curves for the 100 lowest-misfit trial models from each LN parameterization (500 models total); the range of misfit values for the 100 best models from each parameterization is shown in brackets in legend; (b) the 500 inversion-derived V_S profiles shown with true V_S profile and lognormal median $\pm\sigma_{\ln}$ of statistical layer boundaries identified by the DeltaVs method; (c) the average change in $\delta V_{S,\text{avg}}$ with depth and depth ranges used to determine layer boundaries shown in (b); and (d) the median V_S profiles for each LN parameterization, true V_S profile, and DeltaVs median profile derived from 100 lowest-misfit trial models from parameterization based on the DeltaVs results.

an instrumented sledgehammer. With the linear array running from 0 to 94 m, sources were located off both ends of the array at −40, −20, −10, −5, 100, and 150 m. The surface wave data were processed using the workflow and open-source SWprocess Python package developed by Vantassel and Cox (2022), which enables developing experimental surface wave dispersion data with robust measures of uncertainty based on factors such as multiple source types and source locations. The extracted experimental dispersion data were determined to contain contributions from both the fundamental (R0) and first-higher (R1) Rayleigh modes, and classified accordingly [Fig. 8(a)]. The dispersion data were then inverted using Dinver following the same SWinvert workflow and procedures used for the synthetic models. A total of six layering parameterizations were used with LN = 3, 4, 5, 7, 9, and 14, and with $h_{\min} = 1.1$ m and $d_{res} = 30$ m obtained from the R0 experimental dispersion data. After inversion, the LN = 3 parameterization results were rejected from further consideration, as the theoretical dispersion curves did not acceptably fit both the R0 and R1 dispersion data.

The inversion results for all other LN parameterizations are shown in Fig. 8(b), along with the statistical layer boundaries identified by the DeltaVs method. The δV_S profile for Hornsby Bend [Fig. 8(c)] clearly shows three distinct peaks, with depth ranges of 1.75–4.05, 4.05–9.35, and 16.95–27.05 m. The first statistical layer boundary has a lognormal median and a standard deviation of 2.83 m and 0.12, respectively. The second statistical layer boundary has a lognormal median and a standard deviation of 6.94 m and 0.19, respectively. The third statistical layer boundary has a lognormal median and a standard deviation of 21.99 m and 0.11, respectively. The median V_S profiles for each LN parameterization are shown in Fig. 8(d). Three moderate velocity contrasts can be observed in most of them, although these velocity contrasts occur a different depths depending on the parameterization. Based on the number of significant layer boundaries identified by the DeltaVs method, an analyst can reasonably decide to use just the LN = 4 median V_S profile, or some subset of lowest-misfit profiles from that parameterization, to best represent the site. Or the analyst can perform new inversions with layering constrained by the DeltaVs method's results. To demonstrate this, a DeltaVs median profile was developed for Hornsby Bend using the same procedure described for the synthetic ground models and shown in Fig. 8(d). This new profile agrees quite well with the median profiles from the initial LN parameterizations, showing the same three velocity contrasts at slightly variable depths. Resulting from rigorous inversion techniques and a high-quality layering parameterization constrained by the DeltaVs results, the DeltaVs median profile is the most reasonable representation of the subsurface conditions at Hornsby Bend. In order to verify this conclusion and evaluate the efficacy of the DeltaVs method, it is important to make comparisons with actual subsurface layering at the site.

CPT was performed at the Hornsby Bend site to help infer true layer boundaries, and their spatial variability, beneath the 94-m-long surface wave array. CPT was performed along the same line as the MASW array at 0-, 25-, 50-, 75-, and 100-m locations. Collecting invasive data at multiple points along the array is critical for evaluating the spatial variability of subsurface conditions at the site and its effect on the 1D inversion results. For each sounding, the method developed by Robertson (2009) was used to classify the subsurface materials based on the normalized soil behavior type index (I_c). These classifications, as well as the tip resistance (q_c), are shown for all five soundings in Figs. 9(a–e). The subsurface conditions vary beneath the array, with the three farthest soundings (50, 75, and 100 m) showing more clean sand materials with elevated tip resistance at depths <4 m that are not found in the nearer locations (0 and 25 m). Even with this spatial variability, based on the soil behavior type classifications, the subsurface lithology can reasonably be approximated as a three-layer system

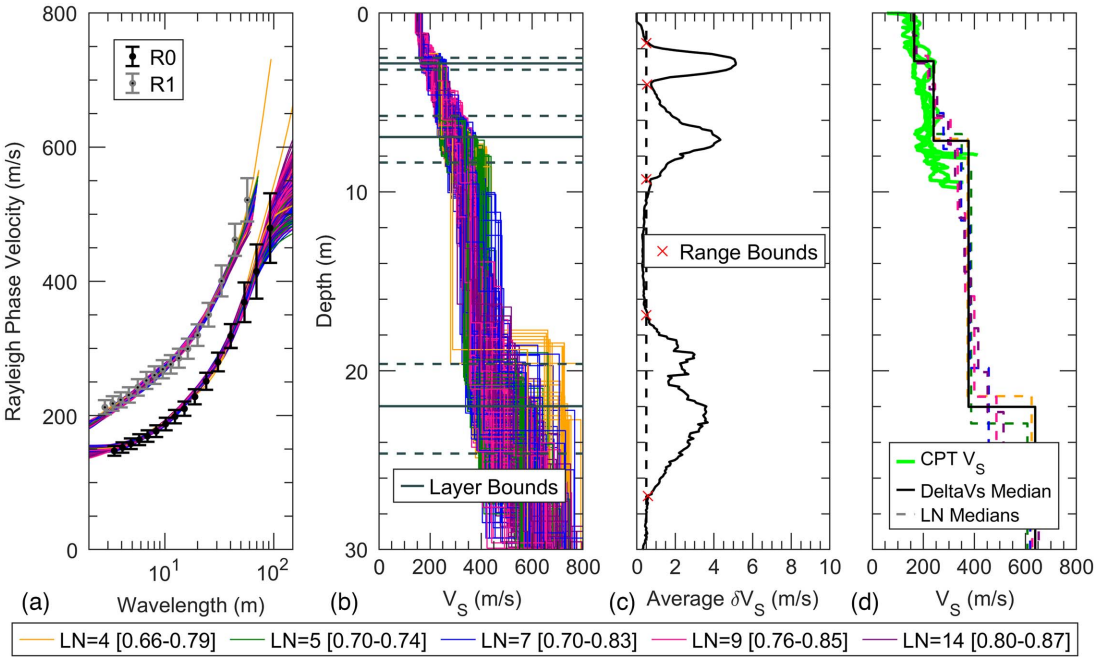

Fig. 8. Summary of inversion results for Hornsby Bend: (a) the R0 and R1 experimental dispersion data and inversion-derived theoretical dispersion curves for the 100 lowest-misfit trial models from each LN parameterization (500 models total); the range of misfit values for the 100 best models from each parameterization is shown in brackets in legend; (b) the 500 inversion-derived V_S profiles shown with lognormal median $\pm\sigma_{\ln}$ of statistical layer boundaries identified by the DeltaVs method; (c) the average change in $\delta V_{S,\text{avg}}$ with depth and depth ranges used to determine layer boundaries shown in (b); and (d) the median V_S profiles for each LN parameterization, V_S profiles from 5 CPT correlations, and DeltaVs median profile derived from 100 lowest-misfit trial models from parameterization based on the DeltaVs results.

J. Geotech. Geoenviron. Eng., 2023, 149(2): 04022126

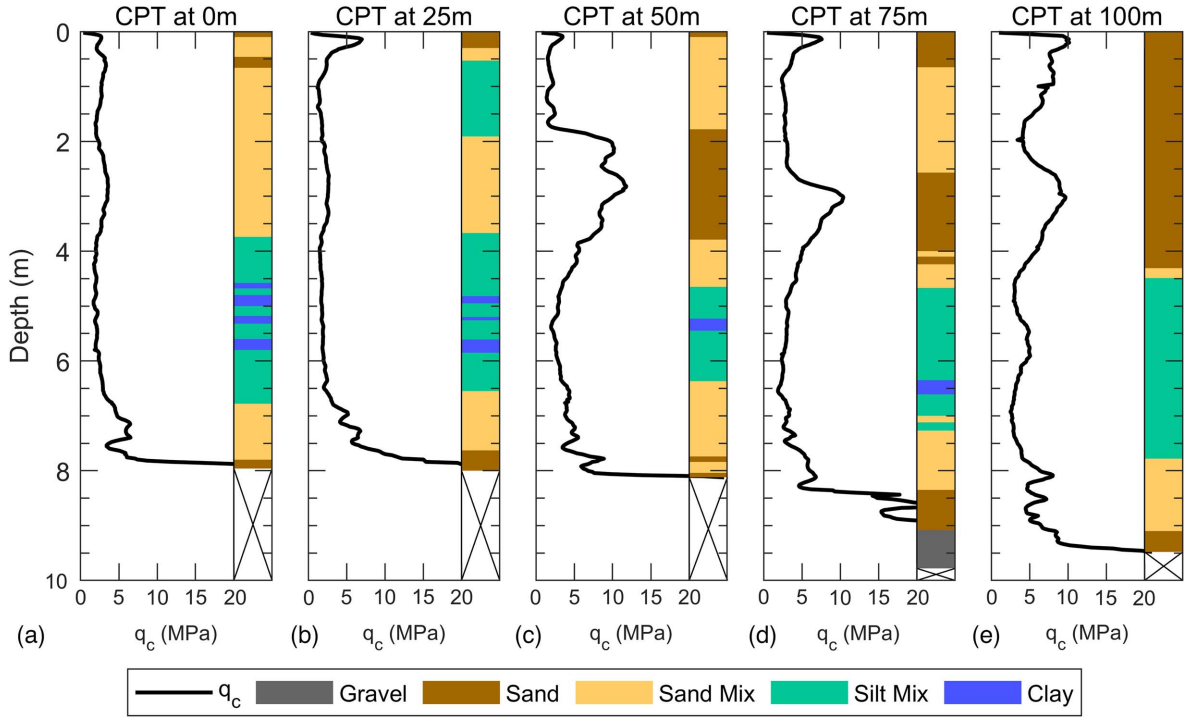

Fig. 9. Tip resistance (q_c) and soil behavior type classification for the CPT tests performed at (a) 0 m; (b) 25 m; (c) 50 m; (d) 75 m; and (e) 100 m along the MASW array at Hornsby Bend.

down to 10 m depth, with conditions alternating between granular material (sands and sand mixes), cohesive material (silt mixes and clays), and then granular material again before CPT refusal. However, it is important to note that a change in material type does not necessarily indicate the presence of a velocity contrast.

In order to make a more direct comparison between the DeltaVs results and the CPT soundings, a correlated V_S profile was developed for each sounding using the average of three CPT-to-V_S correlations (Andrus et al. 2007; Mayne 2007; Robertson 2009), as recommended by Wair et al. (2012). These five correlated V_S profiles are shown together with the inverted median V_S profiles in Fig. 8(d). In general, it can be observed that the five correlated V_S profiles agree quite well with the 1D inverted V_S profiles; however, a more in-depth comparison is needed to judge how well the statistical layer boundaries identified by the DeltaVs method agree with the spatial variability of V_S layer boundaries determined from the CPT-to-V_S correlations. As such, the five correlated V_S profiles are plotted individually in Figs. 10(a–e) for the CPT soundings at 0, 25, 50, 75, and 100 m, respectively. Also shown in Figs. 10(a–e) are (1) the DeltaVs median V_S profile determined from the new inversion performed with layering informed by the DeltaVs results, and (2) 1D statistical representations ($\pm\sigma_{\ln}$ bounds) of the V_S profile beneath the array that were obtained from all of the surface wave inversion results generated using the original acceptable LN parameterizations. The layer bounds shown in blue are the statistical depth bounds identified by the DeltaVs method and originally shown in Fig. 8(b). The V_S bounds shown in red were developed based on all of the V_S values between the statistical depth medians identified by the DeltaVs method. As can be seen, the V_S profiles from the CPT-to-V_S correlations agree quite well with the DeltaVs median profile and the statistical depth and V_S bounds obtained from the inversion results, despite the CPT soundings indicating spatial variability in V_S and depth of refusal ranging from approximately 8–10 m across the site.

The depths of CPT refusal were 7.96, 7.99, 8.12, 9.78, and 9.47 m at the 0-, 25-, 50-, 75-, and 100-m locations, respectively. A 1D method like MASW can only provide average properties and layering within the bounds of the array, but the statistical representation of the subsurface developed from the DeltaVs layer boundaries adequately captures the variability in the depths of refusal for the first three CPT locations, which fall within one standard deviation of the identified lognormal median boundary at 7.02 m. Additionally, the CPT refusal depths for the soundings at 75 and 100 m (i.e., 9.78 and 9.47 m) fall within two standard deviations of the median. This example illustrates the importance of using a method like DeltaVs to obtain both a median or, most likely, 1D representation of the layering beneath a surface wave array as well as some uncertainty bounds that help reflect potential subsurface variability. The CPT data also indicate some lateral variability over the top several meters rather than a single, coherent boundary at the depth of the first layer identified using the DeltaVs method (i.e., 2.86 m). However, this first statistical layer boundary and the DeltaVs median profile agree very well with an increase in correlated V_S for the CPT soundings at 50, 75, and 100 m.

Overall, the top two layer boundaries out of the three boundaries identified by the DeltaVs method at Hornsby Bend appear to correspond well to real velocity contrasts and their spatial variability across the subsurface. Unfortunately, the CPT soundings at the site could not penetrate deep enough to verify the presence of the third layer boundary identified at approximately 22 m. However, boreholes in the general vicinity of the site are known to encounter a shale formation at greater depths, and plans are currently under way to advance boreholes along the array in an attempt to verify the presence and depth of the shale layer so that further comparisons can be made with the DeltaVs method's results. Nonetheless, this example shows that the statistical layer boundaries identified by the DeltaVs method can be used to refine surface wave inversion results and reduce epistemic uncertainty associated with numerous acceptable layering

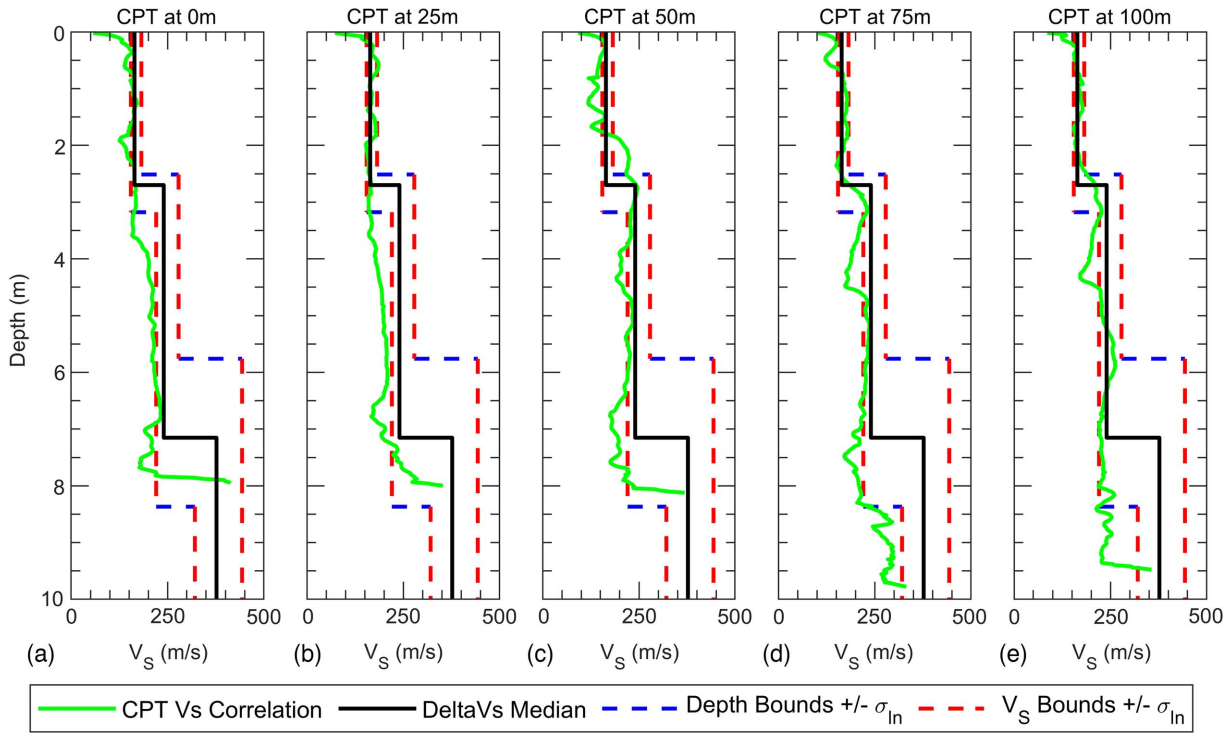

Fig. 10. Correlated V_S profiles for the CPT tests performed at (a) 0 m; (b) 25 m; (c) 50 m; (d) 75 m; and (e) 100 m along the MASW array at Hornsby Bend [(a–e) lognormal median $\pm\sigma_{\ln}$ of statistical layer boundaries identified by the DeltaVs method, lognormal median $\pm\sigma_{\ln}$ of V_S values in between, and DeltaVs median profile shown for comparison].

parameterizations, while still capturing uncertainty that is consistent with the spatial variability across the extent of the array.

Conclusions

Surface wave testing is a powerful tool for noninvasive seismic site characterization; however, when data processing and inversions are performed rigorously in an attempt to accurately identify and account for uncertainty, a significant number of nonunique V_S profiles can be generated. The DeltaVs method provides analysts with a statistical methodology for utilizing these nonunique profiles for estimating the quantity and depth of significant layer boundaries at a site. This information can then be used to inform subsequent analysis and design, or to refine additional inversions as a means to reduce epistemic uncertainty in the derived layer boundaries. The DeltaVs method showed promising results when applied to many of the 12 synthetic ground models tested here. Specifically, it successfully identified and accurately located all layer boundaries for the six synthetic models containing either two or three layers. For the more complex synthetic models containing five or seven layers, the DeltaVs method accurately identified many of the layer boundaries with impedance contrasts greater than 1.5, provided these layers were sufficiently separated from each other as a function of depth, and provided they were located at depths less than approximately $d_{res}/2$, with $d_{res} = \lambda_{\max}/3$. These conditions also appear to affect whether individual layer boundaries in the synthetic ground models have a distinct impact on the shape of the corresponding dispersion data and, by extension, its nonuniqueness.

While the DeltaVs method cannot conclusively determine the quantity or location of all significant layer boundaries for the complex synthetic examples, the information it provides can still shed light on conditions that are likely to exist beneath the array. For example, if the δV_S profile indicates no clear peaks but rather depth ranges where broad and flat areas of elevated δV_S values exist, it is likely that (1) strong impedance contrasts do not exist beneath the array, (2) layer boundaries are too close to distinctly separate/resolve using surface wave methods, or (3) the site is potentially complex, with layering beneath the array that is laterally variable. Further synthetic studies of the complex factors affecting layer identification, including layer depth, layer separation, impedance contrast, and dispersion bandwidth, will provide improved guidance on when the DeltaVs method can be reliably applied. In the meantime, the method can be tested on inversion results without any ill effects; if the δV_S profile indicates strong, distinct peaks then it is likely that significant layer boundaries are present near those depths and this information can be used to reduce epistemic uncertainty using the methods discussed here. However, if the peaks are broad or extend over significant depth ranges, one must acknowledge that epistemic uncertainty in layering cannot be reduced without collecting additional invasive information at the site.

The DeltaVs method was further validated by applying it to real surface wave data collected at the Hornsby Bend site and by considering the spatial variability of layering at the site obtained from five CPT soundings across the array. The DeltaVs method successfully identified two layer boundaries that correspond well with real velocity contrasts and their spatial variability across the array, while a third, deeper layer boundary could not be conclusively established by the CPT data because of its location being greater than the depth of refusal. Further trial application of the DeltaVs method to field sites with supporting information from invasive testing will help to more rigorously assess the method's efficacy. While not yet perfect for identifying all subsurface layers without the aid of a priori information, the DeltaVs method is a simple approach that works in many cases and can help analysts better interpret the nonunique results from surface wave inversions that attempt to rigorously account for uncertainty.

Data Availability Statement

Some or all data, models, or code that support the findings of this study are available from the corresponding author upon reasonable request. The surface wave inversion benchmarks developed by Vantassel and Cox (2020) are publicly available through the DesignSafe-CI. The subsurface models developed during this study are available upon reasonable request from the corresponding author.

Acknowledgments

This work was supported by the US National Science Foundation (NSF) Graduate Research Fellowship under Grant Nos. DGE-2137420, CMMI-2037900, and CMMI-1931162. However, any opinions, findings, and conclusions or recommendations expressed in this material are those of the authors and do not necessarily reflect the views of NSF. Special thanks to Dr. Kevin Anderson at the Austin Water Center for Environmental Research for access to the Hornsby Bend Biosolids Management Plant test site.

References

Andrus, R. D., N. P. Mohanan, P. Piratheepan, B. S. Ellis, and T. L. Holzer. 2007. "Predicting shear-wave velocity from cone penetration resistance." In Vol. 2528 of *Proc., 4th Int. Conf. on Earthquake Geotechnical Engineering*. London: International Society for Soil Mechanics and Geotechnical Engineering.

Baise, L. G., J. Kaklamanos, B. M. Berry, and E. M. Thompson. 2016. "Soil amplification with a strong impedance contrast: Boston, Massachusetts." *Eng. Geol.* 202 (Mar): 1–13. https://doi.org/10.1016/j.enggeo.2015.12.016.

Cox, B. R., and D. P. Teague. 2016. "Layering ratios: A systematic approach to the inversion of surface wave data in the absence of a priori information." *Geophys. J. Int.* 207 (1): 422–438. https://doi.org/10.1093/gji/ggw282.

Cox, B. R., and C. M. Wood. 2011. "Surface wave benchmarking exercise: Methodologies, results, and uncertainties." In *Geo-Risk 2011: Risk Assessment and Management*, 845–852. Reston VA: ASCE.

Cox, B. R., C. M. Wood, and D. P. Teague. 2014. "Synthesis of the UTexas1 surface wave dataset blind-analysis study: Inter-analyst dispersion and shear wave velocity uncertainty." In *Geo-Congress 2014: Geo-Characterization and Modeling for Sustainability*, 850–859. Reston VA: ASCE.

Crocker, J. A., J. P. Vantassel, U. Arslan, and B. R. Cox. 2021. "Limitations of the multichannel analysis of surface waves (MASW) method for subsurface anomaly detection." In *Proc., 6th Int. Conf. on Geotechnical and Geophysical Site Characterization*. London: International Society for Soil Mechanics and Geotechnical Engineering.

Dal Moro, G., S. S. Moustafa, and N. S. Al-Arifi. 2018. "Improved holistic analysis of Rayleigh waves for single-and multi-offset data: Joint inversion of Rayleigh-wave particle motion and vertical- and radial-component velocity spectra." *Pure Appl. Geophys.* 175 (1): 67–88. https://doi.org/10.1007/s00024-017-1694-8.

Di Giulio, G., A. Savvaidis, M. Ohrnberger, M. Wathelet, C. Cornou, B. Knapmeyer-Endrun, F. Renalier, N. Theodoulidis, and P. Y. Bard. 2012. "Exploring the model space and ranking a best class of models in surface-wave dispersion inversion: Application at European strong-motion sites." *Geophysics* 77 (3): B147–B166. https://doi.org/10.1190/geo2011-0116.1.

Fairchild, G. M., J. W. Lane, E. B. Voytek, and D. R. LeBlanc. 2013. "Bedrock topography of western Cape Cod, Massachusetts, based on bedrock altitudes from geologic borings and analysis of ambient seismic noise by the horizontal-to-vertical spectral-ratio method." *US Geol. Surv. Sci. Invest. Map* 3233 (1): 17.

Foti, S., C. Comina, D. Boiero, and L. V. Socco. 2009. "Non-uniqueness in surface-wave inversion and consequences on seismic site response analyses." *Soil Dyn. Earthquake Eng.* 29 (6): 982–993. https://doi.org/10.1016/j.soildyn.2008.11.004.

Foti, S., C. G. Lai, G. J. Rix, and C. Strobbia. 2015. *Surface wave methods for near-surface site characterization*. Boca Raton, FL: CRC Press.

Garofalo, F., et al. 2016a. "InterPACIFIC project: Comparison of invasive and non-invasive methods for seismic site characterization. Part I: Intra-comparison of surface wave methods." *Soil Dyn. Earthquake Eng.* 82 (Mar): 222–240. https://doi.org/10.1016/j.soildyn.2015.12.010.

Garofalo, F., et al. 2016b. "InterPACIFIC project: Comparison of invasive and non-invasive methods for seismic site characterization. Part II: Inter-comparison between surface-wave and borehole methods." *Soil Dyn. Earthquake Eng.* 82 (Mar): 241–254. https://doi.org/10.1016/j.soildyn.2015.12.009.

Griffiths, S. C., B. R. Cox, E. M. Rathje, and D. P. Teague. 2016. "Surface-wave dispersion approach for evaluating statistical models that account for shear-wave velocity uncertainty." *J. Geotech. Geoenviron. Eng.* 142 (11): 04016061. https://doi.org/10.1061/(ASCE)GT.1943-5606.0001552.

Haskell, N. A. 1953. "The dispersion of surface waves on multilayered media." *Bull. Seismol. Soc. Am.* 43 (1): 17–34. https://doi.org/10.1785/BSSA0430010017.

Hollender, F., et al. 2018. "Characterization of site conditions (soil class, V S30, velocity profiles) for 33 stations from the French permanent accelerometric network (RAP) using surface-wave methods." *Bull. Earthquake Eng.* 16 (6): 2337–2365. https://doi.org/10.1007/s10518-017-0135-5.

Kaklamanos, J., and B. A. Bradley. 2018. "Challenges in predicting seismic site response with 1D analyses: Conclusions from 114 KiK-net vertical seismometer arrays challenges in predicting seismic site response with 1D analyses." *Bull. Seismol. Soc. Am.* 108 (5A): 2816–2838. https://doi.org/10.1785/0120180062.

Kayen, R., R. E. S. Moss, E. M. Thompson, R. B. Seed, K. O. Cetin, A. Der Kiureghian, Y. Tanaka, and K. Tokimatsu. 2013. "Shear-wave velocity–based probabilistic and deterministic assessment of seismic soil liquefaction potential." *J. Geotech. Geoenviron. Eng.* 139 (3): 407. https://doi.org/10.1061/(ASCE)GT.1943-5606.0000743.

Lai, C. G., S. Foti, and G. J. Rix. 2005. "Propagation of data uncertainty in surface wave inversion." *J. Environ. Eng. Geophys.* 10 (2): 219–228. https://doi.org/10.2113/JEEG10.2.219.

Mayne, P. W. 2007. "In-situ test calibrations for evaluating soil parameters." In Vol. 3 of *Characterization & engineering properties of natural soils*, 1601–1652. London: Taylor & Francis.

Nocedal, J., and S. Wright. 2006. *Numerical optimization*. New York: Springer.

Park, C. B., R. D. Miller, and J. Xia. 1999. "Multichannel analysis of surface waves." *Geophysics* 64 (3): 800–808. https://doi.org/10.1190/1.1444590.

Pei, D., J. N. Louie, and S. K. Pullammanappallil. 2007. "Application of simulated annealing inversion on high-frequency fundamental-mode Rayleigh wave dispersion curves." *Geophysics* 72 (5): R77–R85. https://doi.org/10.1190/1.2752529.

Pratt, T. L., and L. S. Schleicher. 2021. "Characterizing ground-motion amplification by extensive flat-lying sediments: The seismic response of the eastern US Atlantic Coastal Plain strata." *Bull. Seismol. Soc. Am.* 111 (4): 1795–1823. https://doi.org/10.1785/0120200328.

Ramírez-Guzmán, L., O. S. Boyd, S. Hartzell, and R. A. Williams. 2012. "Seismic velocity model of the central United States (version 1): Description and simulation of the 18 April 2008 Mt. Carmel, Illinois, earthquake." *Bull. Seismol. Soc. Am.* 102 (6): 2622–2645. https://doi.org/10.1785/0120110303.

Robertson, P. K. 2009. "Interpretation of cone penetration tests—A unified approach." *Can. Geotech. J.* 46 (11): 1337–1355. https://doi.org/10.1139/T09-065.

Sambridge, M. 1999a. "Geophysical inversion with a neighbourhood algorithm—I. Searching a parameter space." *Geophys. J. Int.* 138 (2): 479–494. https://doi.org/10.1046/j.1365-246X.1999.00876.x.

Sambridge, M. 1999b. "Geophysical inversion with a neighbourhood algorithm—II. Appraising the ensemble." *Geophys. J. Int.* 138 (3): 727–746. https://doi.org/10.1046/j.1365-246x.1999.00900.x.

Shaw, J. H., et al. 2015. "Unified structural representation of the southern California crust and upper mantle." *Earth Planet. Sci. Lett.* 415 (Apr): 1–15. https://doi.org/10.1016/j.epsl.2015.01.016.

Shible, H., A. Laurendeau, P. Y. Bard, and F. Hollender. 2018. "Importance of local scattering in high frequency motion: Lessons from interpacific project sites, application to the KiK-net database and derivation of new hard-rock GMPE." In *Proc., 16th European Conf. on Earthquake Engineering*, 18–21. Istanbul, Turkey: European Association for Earthquake Engineering.

Socco, L. V., and D. Boiero. 2008. "Improved Monte Carlo inversion of surface wave data." *Geophys. Prospect.* 56 (3): 357–371. https://doi.org/10.1111/j.1365-2478.2007.00678.x.

Socco, L. V., S. Foti, and D. Boiero. 2010. "Surface-wave analysis for building near-surface velocity models—Established approaches and new perspectives." *Geophysics* 75 (5): 75A83–75A102. https://doi.org/10.1190/1.3479491.

Stokoe, K. H., B. R. Cox, P. Clayton, and F. Menq. 2020. "NHERI@U-Texas experimental facility with large-scale mobile shakers for field studies." *Front. Built Environ.* 6 (Nov): 575973. https://doi.org/10.3389/fbuil.2020.575973.

Teague, D., B. Cox, B. Bradley, and L. Wotherspoon. 2018. "Development of deep shear wave velocity profiles with estimates of uncertainty in the complex interbedded geology of Christchurch, New Zealand." *Earthquake Spectra* 34 (2): 639–672. https://doi.org/10.1193/041117EQS069M.

Teague, D. P., and B. R. Cox. 2016. "Site response implications associated with using non-unique Vs profiles from surface wave inversion in comparison with other commonly used methods of accounting for Vs uncertainty." *Soil Dyn. Earthquake Eng.* 91 (Dec): 87–103. https://doi.org/10.1016/j.soildyn.2016.07.028.

Thabet, M. 2019. "Site-specific relationships between bedrock depth and HVSR fundamental resonance frequency using KiK-NET data from Japan." *Pure Appl. Geophys.* 176 (11): 4809–4831. https://doi.org/10.1007/s00024-019-02256-7.

Thomson, W. T. 1950. "Transmission of elastic waves through a stratified solid medium." *J. Appl. Phys.* 21 (2): 89–93. https://doi.org/10.1063/1.1699629.

Vantassel, J. P., and B. R. Cox. 2020. *Surface wave inversion benchmarks*. Miami: DesignSafe-CI. https://doi.org/10.17603/ds2-cpmr-v194.

Vantassel, J. P., and B. R. Cox. 2021a. "A procedure for developing uncertainty-consistent Vs profiles from inversion of surface wave dispersion data." *Soil Dyn. Earthquake Eng.* 145 (Jun): 106622. https://doi.org/10.1016/j.soildyn.2021.106622.

Vantassel, J. P., and B. R. Cox. 2021b. "SWinvert: A workflow for performing rigorous 1-D surface wave inversions." *Geophys. J. Int.* 224 (2): 1141–1156. https://doi.org/10.1093/gji/ggaa426.

Vantassel, J. P., and B. R. Cox. 2022. "SWprocess: A workflow for developing robust estimates of surface wave dispersion uncertainty." *J. Seismol.* 26: 731–756. https://doi.org/10.1007/s10950-021-10035-y.

Wair, B. R., J. T. DeJong, and T. Shantz. 2012. *Guidelines for estimation of shear wave velocity profiles*. Berkeley, CA: Pacific Earthquake Engineering Research Center.

Wathelet, M. 2008. "An improved neighborhood algorithm: Parameter conditions and dynamic scaling." *Geophys. Res. Lett.* 35 (9). https://doi.org/10.1029/2008GL033256.

Wathelet, M., J. L. Chatelain, C. Cornou, G. D. Giulio, B. Guillier, M. Ohrnberger, and A. Savvaidis. 2020. "Geopsy: A user-friendly open-source tool set for ambient vibration processing." *Seismol. Res. Lett.* 91 (3): 1878–1889. https://doi.org/10.1785/0220190360.

Wathelet, M., D. Jongmans, and M. Ohrnberger. 2004. "Surface-wave inversion using a direct search algorithm and its application to ambient vibration measurements." *Near Surf. Geophys.* 2 (4): 211–221. https://doi.org/10.3997/1873-0604.2004018.

Wathelet, M., D. Jongmans, and M. Ohrnberger. 2005. "Direct inversion of spatial autocorrelation curves with the neighborhood algorithm." *Bull. Seismol. Soc. Am.* 95 (5): 1787–1800. https://doi.org/10.1785/0120040220.

Yamanaka, H., and H. Ishida. 1996. "Application of genetic algorithms to an inversion of surface-wave dispersion data." *Bull. Seismol. Soc. Am.* 86 (2): 436–444. https://doi.org/10.1785/BSSA0860020436.

Yong, A., A. Martin, K. Stokoe, and J. Diehl. 2013. *ARRA-funded VS30 measurements using multi-technique approach at strong-motion stations in California and central-eastern United States.* USGS Open-File Rep. No. 2013-1102. Washington, DC: USGS.

Yust, M. B., B. R. Cox, and T. Cheng. 2018. "Epistemic uncertainty in Vs profiles and Vs30 values derived from joint consideration of surface wave and H/V data at the FW07 TexNet station." In *Geotechnical earthquake engineering and soil dynamics V: Seismic hazard analysis, earthquake ground motions, and regional-scale assessment*, 387–399. Reston, VA: ASCE.

Yust, M. B. S. 2018. "Dynamic site characterization of TexNet ground motion stations." Master's thesis, Dept. of Civil, Architectural, and Environmental Engineering, Univ. of Texas at Austin.

Zywicki, D. J. 1999. *Advanced signal processing methods applied to engineering analysis of seismic surface waves*. Atlanta: Georgia Institute of Technology.